Atmospheric Environment 128 (2016) 208–215

Contents lists available at ScienceDirect

Atmospheric Environment

journal homepage: www.elsevier.com/locate/atmosenv

Valley heat deficit as a bulk measure of wintertime particulate air pollution in the Arve River Valley

Charles Chemel [a, *], Gabriele Arduini [b, c], Chantal Staquet [b], Yann Largeron [d], Dominique Legain [d], Diane Tzanos [d], Alexandre Paci [d]

[a] National Centre for Atmospheric Science (NCAS), Centre for Atmospheric & Instrumentation Research, University of Hertfordshire, College Lane, Hatfield, AL10 9AB, UK

[b] Université Grenoble Alpes, Laboratoire des Ecoulements Géophysiques et Industriels (LEGI, UMR 5519 UJF/CNRS/Grenoble INP), F-38000 Grenoble, France

[c] Centre for Atmospheric & Instrumentation Research, University of Hertfordshire, College Lane, Hatfield, AL10 9AB, UK

[d] Centre National de Recherches Météorologiques, Groupe d'étude de l'Atmosphère Météorologique (CNRM-GAME, UMR 3589 Météo-France and CNRS), 42 Avenue Gaspard Coriolis, 31057 Toulouse Cedex 1, France

HIGHLIGHTS

- Cold-air pools lead to severe air pollution episodes in the Arve River Valley.
- We examine the temporal variability of PM_{10} concentration.
- It is largely explained by that of the valley heat deficit on a daily time scale.
- Emissions and local dynamics play a major role on an hourly time scale.

ARTICLE INFO

Article history:
Received 24 June 2015
Received in revised form
22 December 2015
Accepted 23 December 2015
Available online 29 December 2015

Keywords:
PM_{10}
Temperature inversions
Drainage flows

ABSTRACT

Urbanized valleys are particularly vulnerable to particulate air pollution during the winter, when ground-based stable layers or cold-air pools persist over the valley floor. We examine whether the temporal variability of PM_{10} concentration in the section of the Arve River Valley between Cluses and Servoz in the French Alps can be explained by the temporal variability of the valley heat deficit, a bulk measure of atmospheric stability within the valley. We do this on the basis of temperature profile and ground-based PM_{10} concentration data collected during wintertime with a temporal resolution of 1 h or finer, as part of the Passy-2015 field campaign conducted around Passy in this section of valley. The valley heat deficit was highly correlated with PM_{10} concentration on a daily time scale. The hourly variability of PM_{10} concentrations was more complex and cannot be explained solely by the hourly variability of the valley heat deficit. The interplay of the diurnal cycles of emissions and local dynamics is demonstrated and a drainage mechanism for observed nocturnal dilution of near-surface PM_{10} concentrations is proposed.

1. Introduction

Urbanized valleys often experience severe air pollution events during the winter, when a cold-air pool (CAP) lingers over the valley floor (e.g. Chazette et al., 2005; Malek et al., 2006; de Franceschi and Zardi, 2009; Gohm et al., 2009; Harnisch et al., 2009; Schnitzhofer et al., 2009; Silcox et al., 2012). These CAPs are characterized by a strongly stratified ground-based temperature inversion, thereby suppressing vertical mixing of pollutants and decoupling the valley atmosphere from the generally stronger winds aloft, and can persist for multiple days, leading to an accumulation of pollution. These accumulations lead to PM_{10} (suspended particulate matter with aerodynamic diameters less than 10 μm) concentrations that exceed the daily average limit value of 50 μg m^{-3} required by the European Directive 2008/50/EC on ambient air quality and cleaner air for Europe not to be exceeded for more than 35 days in a calendar year. As an illustration of the extent of the problem, in Passy in the Arve River Valley in the French Alps, the number of days in a calendar year during which PM_{10} concentrations exceeded the daily average limit value of

* Corresponding author.
E-mail address: c.chemel@herts.ac.uk (C. Chemel).

http://dx.doi.org/10.1016/j.atmosenv.2015.12.058

50 μg m^{-3} has been greater than 35 days since the monitoring site was installed in 2007. This part of the Arve River Valley concentrates a mix of PM_{10} emission sources, including residential (wood) combustion, road transport with a major international route to Italy and industries, which contribute to elevated PM_{10} concentrations in stagnant CAPs. This problem is not isolated and is a major concern in complex terrain across the world (see for instance Green et al., 2015; for western US valleys), although legislation regarding pollution levels varies from country to country.

Previous works investigated relationships between wintertime particulate air pollution and meteorological variables in western US valleys. Silcox et al. (2012) related wintertime daily average $PM_{2.5}$ concentrations measured in the Salt Lake Valley, Utah, USA, during the Persistent Cold-Air Pool Study (PCAPS, Lareau et al., 2013), to the valley heat deficit, a bulk measure of atmospheric stability within the valley, calculated using data from rawinsondes (RS) launched daily at 1200 UTC [0500 local time (LT)] from the Salt Lake City International Airport. Daily average $PM_{2.5}$ concentrations were found well correlated and to increase with the valley heat deficit calculated at 0500 LT, which increased from day to day during persistent CAPs. The squared Pearson product-moment correlation coefficient r^2 was 0.61 (based on a linear regression of the data presented in their Fig. 3). However, this strong relationship manifested mostly as an association between low values of $PM_{2.5}$ concentrations and valley heat deficit.

Whiteman et al. (2014) extended this work and provided context for PCAPS by examining relationships between wintertime meteorological conditions and particulate air pollution in the Salt Lake Valley using data from twice-daily RS launched at 0000 and 1200 UTC (1700 and 0500 LT, respectively) from the Salt Lake City International Airport and daily average particulate air pollution measurements over a 40-year period from 1973 to 2003. A close association between $PM_{2.5}$ concentrations and valley heat deficit was found on winter, weekly and daily time scales, for the 15 winter seasons from 1998–1999 to 2012–2013 for which $PM_{2.5}$ concentration data were available. The correlation coefficient r^2 was 0.65 for daily average $PM_{2.5}$ concentrations for the winter seasons 1999–2000 to 2010–2011. Elevated $PM_{2.5}$ concentrations were found to be more likely to occur when snow cover was present, when surface pressure and column-mean valley relative humidity were high, and when column-mean valley temperature and wind speed were low. No statistically significant long-term trend in wintertime atmospheric stability within the valley could be detected in the 40-year record, indicating that the only option to improve air quality in such valleys is to consider stricter emission control strategies.

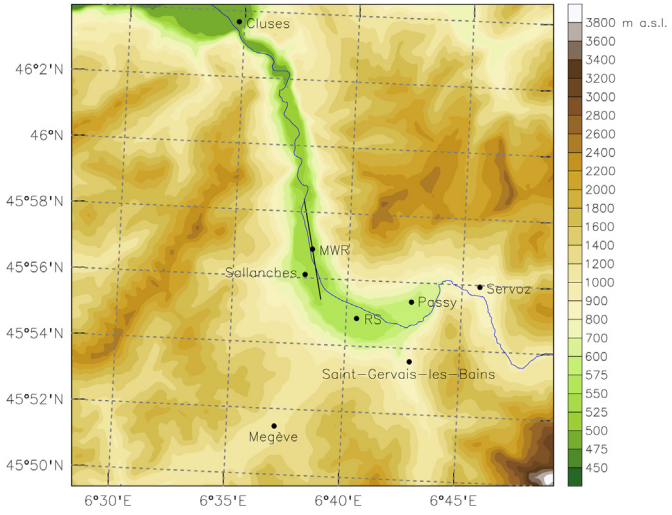

Fig. 1. Topographic map of the section of the Arve River Valley between Cluses and Servoz in the French Alps, displaying the terrain height (filled contours), Arve River (blue line) and location of the PM_{10} monitoring site in Sallanches, and of the rawinsonde (RS) and microwave radiometer (MWR) sites. The black line indicates the horizontal direction of the MWR beam, orientated 343° North. (For interpretation of the references to colour in this figure legend, the reader is referred to the web version of this article.)

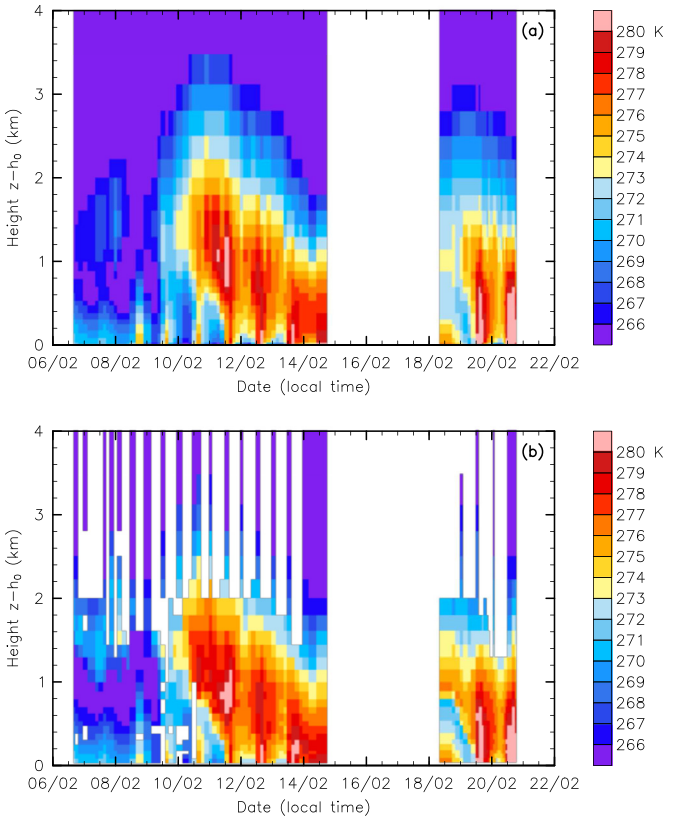

Fig. 2. Temperature profiles above ground level at $z = h_0$ at the location of the microwave radiometer (MWR) site (see Fig. 1 and Table 1), (a) retrieved from the MWR data and (b) from the rawinsonde (RS) ascents during the Passy-2015 intensive observation periods (IOPs) from 6 to 14 February 2015 (IOP1) and from 17 to 20 February 2015 (IOP2) at the times of the RS launches.

Green et al. (2015) examined relationships between daily average $PM_{2.5}$ concentrations and valley heat deficit, or differences between valley floor and ridge top temperatures, during wintertime in five western US valleys (Salt Lake City, Utah; Reno, Nevada; Boise, Idaho; Missoula, Montana; and Spokane, Washington). The valley heat deficit was calculated using data from twice-daily RS launched at 0000 and 1200 UTC (1700 and 0500 LT, respectively, for Salt Lake City, Boise and Missoula, and 1600 and 0400 LT, respectively, for Reno and Spokane) from nearby airports except for Missoula, where RS were not launched. For Missoula, differences between valley floor and ridge top temperatures were considered. $PM_{2.5}$ concentrations were highly correlated with valley heat deficit (or difference between valley and ridge top temperatures for Missoula) for all cities except Spokane, where the RS atmospheric profiles were not representative of the valley atmosphere. For all cities except Spokane, the correlation coefficient r^2 was greater for snow cover days than snow free days and was in the range 0.46–0.53. For a given valley heat deficit (or difference between valley and ridge top temperatures for Missoula) snow cover days experienced higher $PM_{2.5}$ concentrations than snow free days, mainly due to enhanced ammonium nitrate concentrations. This

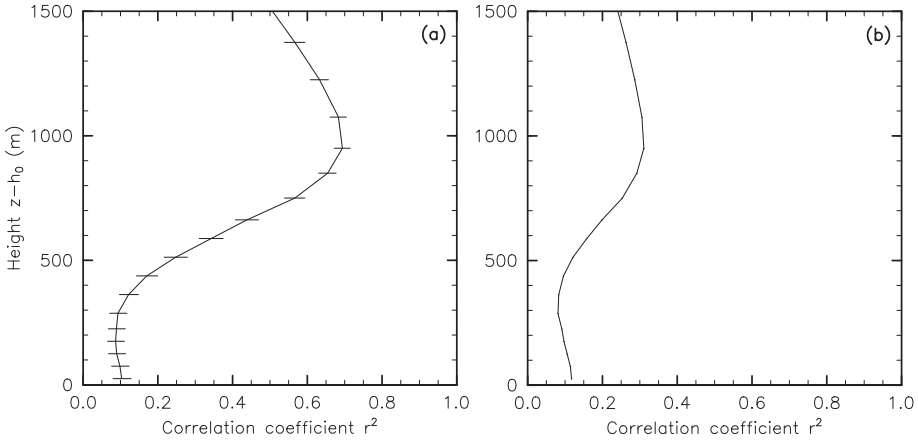

Fig. 3. Squared Pearson product-moment correlation coefficient r^2 between the heat deficit calculated for different integration heights z and PM_{10} concentration at Sallanches during the Passy-2015 field campaign main observation period (from 10 January to 28 February 2015) displayed as a function of height above ground level at $z = h_0$ at the location of the microwave radiometer site (see Fig. 1 and Table 1), on (a) daily and (b) hourly time scales. 95% confidence intervals, determined using the Fisher transformation, are shown as horizontal lines.

increase in ammonium nitrate concentrations is the result of increase secondary formation under higher humidity and lower temperatures on snow cover days. This finding is consistent with that reported by Whiteman et al. (2014) that the probability of exceeding the daily average 35 μg m^{-3} US National Ambient Air Quality Standard in the Salt Lake Valley is roughly 4 times greater when there is snow cover present than when there is no snow cover. Weighting wintertime average $PM_{2.5}$ concentrations by the ratio of the specific winter average valley heat deficit to the long-term winter average valley heat deficit was found to reduce the winter-to-winter variability in $PM_{2.5}$ concentrations, allowing long-term trends to be more clearly identified so as to examine the effectiveness of emission control strategies.

The statistical relationships between daily average $PM_{2.5}$ concentrations and valley heat deficit reported by Silcox et al. (2012), Whiteman et al. (2014) and Green et al. (2015) are limited by the use of daily average values that cannot resolve shorter term variability. This study uses temperature profile and ground-based PM_{10} concentration data collected with a temporal resolution of 1 h or finer, as part of the Passy-2015 field campaign conducted around Passy in the section of the Arve River Valley between Cluses and Servoz in the French Alps during the winter season 2014–2015 (Paci et al., 2015a, b; Staquet et al., 2015), characterized by typical wintertime meteorological conditions (not shown). We analyze the data to investigate.

- whether conclusions from previous works as regards the relationships between daily average particulate air pollution and valley heat deficit are applicable to this section of the Arve River Valley;
- whether the hourly variability of PM_{10} concentrations in this section of the Arve River Valley can be explained by the hourly variability of the valley heat deficit.

The methodology is presented in Sect. 2, results are presented and discussed in Sect. 3, and conclusions are given in Sect. 4.

2. Methodology

In the following the sites and instruments used in this work, namely a microwave radiometer (MWR) and PM_{10} monitor are described. The MWR data were collected during the main observation period of the Passy-2015 field campaign (from 10 January to 28 February 2015). We also use RS data collected during the intensive observation periods (IOPs) of the field campaign to compare to the MWR data.

2.1. Site

A topographic map of the section of the Arve River Valley between Cluses and Servoz in the French Alps is presented in Fig. 1. LT is UTC+1 in the Arve River Valley during wintertime. The average times of sunrise and sunset above the horizon in this section of valley during the Passy-2015 field campaign main observation period were 0743 and 1743 LT, respectively.

This section of valley includes two major towns: Passy and Sallanches, with populations of 11,214 and 15,957 (2012 census), respectively. The valley-floor elevation decreases gradually down-valley from 588 m at Passy to 488 m at Cluses over a distance of 23 km, yielding an average slope of 0.25° between these two points. The width of the valley floor along this section of the valley increases gradually up-valley from just about 200 m at Cluses, where the valley presents a major constriction, to approximately 2000 m near the location of the RS site, and hardly decreases from there towards the escarpment leading to Servoz. Table 1 lists characteristics of the sites for the PM_{10} and meteorological measurements used in this paper and shown in Fig. 1.

2.2. Instruments

A standard Thermo Scientific TEOM™ FDMS (Filter Dynamic Measurement System) sampler, maintained by the Air Rhône-Alpes air quality agency, provided routine hourly PM_{10} concentrations at an urban location in Sallanches.

A scanning Humidity And Temperature PROfiler (HATPRO), manufactured by Radiometer Physics GmbH, was deployed within the perimeter of the airfield in Sallanches. The HATPRO is a MWR measuring brightness temperatures for two 7-channel frequency reception bands: from 22.24 to 31.4 GHz and from 51 to 58 GHz. The first frequency band contains information on cloud liquid water content and the vertical profile of atmospheric absolute humidity, while the second frequency band contains information on the vertical profile of atmospheric temperature. A steerable paraboloid mirror, covered by a microwave transparent radome insures the focussing of the beam (width of 3° or less) and enables radiation from ±90° elevation to be received. The radome was continuously

Table 1
Characteristics of the sites for the PM_{10} and meteorological measurements used in this paper and shown in Fig. 1.

Site name	Latitude	Longitude	Elevation (m)	Instrument
Sallanches	45.93507	6.63556	542	TEOM™ FDMS
Rawinsondes (RS)	45.91400	6.67430	561	Rawinsonde
Microwave radiometer (MWR)	45.94800	6.64008	535	Microwave radiometer

protected by a heated blower system to prevent the formation of dew and any condensation. The MWR was operated in a bilateral two-scan mode providing tropospheric profiles every 9–10 min, with elevation angles ±90.0°, ±42.0°, ±30.0°, ±19.2°, ±10.2°, ±5.4° above the horizon. The MWR beam was orientated 343° North (see Fig. 1). An absolute system calibration, utilizing the built-in ambient temperature target and an external liquid-nitrogen-cooled radiometric target, was performed before the start of the Passy-2015 campaign. Further details on the technical specifications and calibration methods of the HATPRO are given by Rose et al. (2005).

In this work, we use temperature data retrieved from the measured brightness temperatures, following the combined elevation scanning and multiple frequency retrieval method described by Crewell and Löhnert (2007). No long-term routine upper air observations are available for the section of the valley considered herein, so data from RS launched twice a day at 0000 and 1200 UTC (0100 and 1300 LT) at the WMO station 6610 at Payerne, Switzerland, during the period 1994–2014, were used to develop the retrieval algorithms. The station is located in the Broye River Valley between the Jura and Prealps mountain ranges (of mean height above the valley floor similar to that at the location of the MWR) at latitude 46.82°, longitude 6.95° (about 100 km north of the MWR site) and elevation 491 m (similar to that of the MWR site, see Table 1), and has a climate and weather conditions typical of Alpine regions and so similar to that of the valley section considered herein. The retrieval algorithm uses simulated brightness temperatures at required frequencies and elevation angles derived from the pressure, temperature and humidity profiles from the long-term RS dataset via radiative transfer calculations (see for instance Crewell and Löhnert, 2007; Löhnert and Maier, 2012).

Temperature profiles retrieved from the MWR data were compared to the temperature profiles from the RS ascents, using Väisälä RS92 reusable radiosondes (Legain et al., 2013), launched at the RS site during the Passy-2015 IOPs. The RS temperature data were interpolated on the vertical levels of the retrieved MWR data. The time interval between two RS profiles varied from 1.5 to 12 h. Fig. 2 displays times series of temperature profiles retrieved from the MWR data and from the RS ascents during the IOPs (IOP1 from 6 to 14 February 2015 and IOP2 from 17 to 20 February 2015) at the times of the RS launches. The overall temporal variability of the temperature profiles derived from the MWR data is comparable to that of the temperature profiles from the RS ascents. Accuracies reported in terms of root-mean-square-error (RMSE) for temperature for the HATPRO are typically between 0.4 and 0.8 K in the lowest 500 m a.g.l., gradually increasing with height to 1.2 K at 1200 m a.g.l. and 1.7 K at 4000 m a.g.l. (Löhnert and Maier, 2012). Assuming that the atmosphere is horizontally homogeneous in the valley section, we can quantitatively compare the two datasets. This assumption will need to be evaluated in future work, for instance using results from numerical model simulations. The root-mean-square-differences calculated from the two datasets are 0.7 K below 500 m a.g.l., 1.1 K from 500 to 1200 m a.g.l. and 1.7 K from 1200 to 4000 m a.g.l., which are comparable to the typical accuracies (RMSE) for the HATPRO. This result suggests that the vertical structure of the valley atmosphere in terms of temperature is similar above the MWR and RS sites. If this is the case, this indicates that the accuracy of the temperature profiles retrieved from the MWR data (based on long-term observations at Payerne) is as good as the typical accuracy for the HATPRO.

2.3. Bulk measure of atmospheric stability

In the analysis presented in Sect. 3, we use extensively the heat deficit H (Whiteman et al., 1999) as a bulk measure of atmospheric stability, defined by

$$H(z) = c_p \int_{h_0}^{z} \rho(z')[\theta(z) - \theta(z')]dz', \quad (1)$$

where $c_p = 1{,}005$ J kg^{-1} K^{-1} is the specific heat of air at constant pressure, $z-h_0$ is the height above ground level at $z = h_0$, and ρ and θ are the air density and potential temperature, respectively. The heat deficit is the heat (energy) per unit area (in J m^{-2}) required to bring a column of air of unit area and depth $z-h_0$ to the potential temperature at height z (and hence leading to a dry adiabatic lapse rate throughout the column). This method of determining a bulk measure of stability relies on a choice of integration height, as discussed in Sect. 3.

3. Results and discussion

3.1. Temporal variability of PM_{10} concentrations associated with the valley heat deficit

Since the focus of this work is on correlating ground-based PM_{10} concentrations to the heat deficit, we determined the height above ground level at which the correlation coefficient r^2 between the heat deficit and PM_{10} concentration at Sallanches during the Passy-2015 field campaign was maximum. The temperature derived from the MWR data was hourly averaged to correspond to the temporal resolution of the PM_{10} concentration measurements. The heat deficit was calculated to different integration heights at the location of the MWR site from the hourly average temperature profiles, assuming that the valley atmosphere is in hydrostatic balance, as is reasonable (see for instance Rampanelli et al., 2004; Serafin and Zardi, 2011; Arduini et al., 2015). Fig. 3 shows that the correlation coefficient r^2 increases with height, reaching a maximum value for a height above ground level $z-h_0$ near 1000 m, and decreases with height above, on both daily (midnight to midnight LT) and hourly time scales. The integration height corresponding to the maximum correlation is of the order of the mean height of the surrounding mountain ranges at the location of the MWR site (see Fig. 1). This result is consistent with that reported by Whiteman et al. (2014) for the Salt Lake Valley, Utah, USA, and simply indicates that atmospheric stability above the bounding terrain is of decreasing significance for the trapping of pollutants in the valley. In the following the heat deficit integrated to this height will be referred to as valley heat deficit and denoted by H_v. The maximum correlation coefficient is significantly higher for the daily average values ($r^2 = 0.69$) than for the hourly average values ($r^2 = 0.31$). The

correlation coefficient for the daily average values is comparable to those reported for US valleys, which are in the range 0.46–0.65 (see Sect. 1) and for the Grenoble valley in the French Alps ($r^2 = 0.46$; Largeron, 2010; Largeron and Staquet, 2015).

The time series and scatter plot of the daily average valley heat deficit and PM_{10} concentration at Sallanches during the Passy-2015 field campaign main observation period are presented in Fig. 4. We note that all the five days when the daily average PM_{10} concentration exceeded the daily average limit value of 50 μg m^{-3} were associated with persistent CAPs (Whiteman et al., 2001; Lareau et al., 2013) as opposed to diurnal CAPs. Diurnal CAPs are destroyed the next day after sunrise by the growth of a convective boundary layer. In this work, we define persistent CAP events as CAP events triggered by an increase in the daily average valley heat deficit and lasting for as long as the daily average valley heat deficit is above that of the first day of the event. Persistent CAP events were observed during IOP1 (from 8 to 14 February 2015) and IOP2 (from 17 to 20 February 2015). The overall temporal variability of the daily average PM_{10} concentration is comparable to that of the valley heat deficit. There are fairly large hourly variations of both the valley heat deficit and PM_{10} concentration, as indicated by their ranges of variations in Fig. 4a.

The studies by Silcox et al. (2012), Whiteman et al. (2014) and Green et al. (2015) used valley heat deficit values calculated at a particular time of day (either 0400 or 0500 LT). Considering another particular time of day might have led to different relationships between daily average PM_{10} concentration and valley heat deficit. To ascertain whether hourly variations of the valley heat deficit affect the correlation between daily average PM_{10} concentration and valley heat deficit, the correlation coefficients between daily PM_{10} concentration and the valley heat deficit calculated for every hour of day are shown in Fig. 5 and compared to that obtained by considering the daily average value. The correlation coefficient r^2 calculated for every hour of day varies between 0.44 and 0.69. It is the highest and close to that calculated using the daily average valley heat deficit ($r^2 = 0.69$) at 1100 LT, and within 10% of that calculated using the daily average valley heat deficit during the morning hours from 0600 to 1300 LT. In order to maximize the variance of daily average PM_{10} concentration explained by the valley heat deficit calculated at a particular time of day, it is therefore more appropriate to calculate the valley heat deficit during these morning hours, in this valley and most likely in other valleys.

The time series and scatter plot of the hourly average valley heat deficit and PM_{10} concentration at Sallanches are presented in Fig. 6. Not surprisingly, both the hourly valley heat deficit and PM_{10} concentration varies over a wide range of temporal scales. Given the spatial separation of measurement sites and various PM_{10} emission sources, and the time scales of processes involved in changing PM_{10} concentrations and distributing any changes (e.g. emissions, deposition, advection, mixing), out-of-phase variations will weaken direct correlation on an hourly time scale, where a change in one variable in 1 h results in a later or slower change in PM_{10} concentration. In this sense the daily average is arguably a type of 'fuzzy' verification, integrating all sub-diurnal time scales. Single-time-per-day correlations would also be affected, but using all hours would suffer a so called 'double penalty', making them worse. The role of PM_{10} emissions and local dynamics on the hourly variability of PM_{10} concentrations will be examined in the following subsection of the paper.

We note that filtering the data around possible factors can lead to meaningless conclusions since the size of the dataset will be reduced. For example, washout and more generally scavenging by

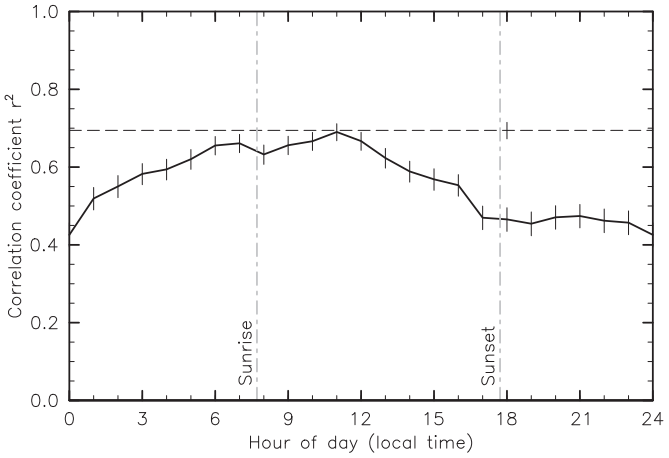

Fig. 5. Squared Pearson product-moment correlation coefficient r^2 between daily PM_{10} concentration and the valley heat deficit at Sallanches calculated for every hour of day (solid line), compared to that obtained by considering the daily average value (dashed line), during the Passy-2015 field campaign main observation period (from 10 January to 28 February 2015). 95% confidence intervals, determined using the Fisher transformation, are shown as black vertical lines. The grey vertical lines show the average times of sunrise and sunset above the horizon during the period considered.

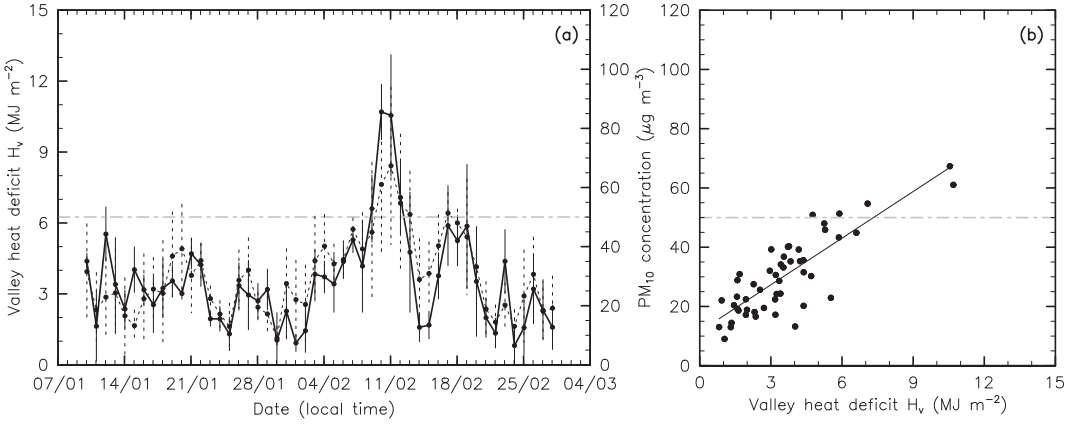

Fig. 4. (a) Time series of the daily average valley heat deficit (solid line) and PM_{10} concentration (dotted line) at Sallanches and (b) corresponding scatter plot, during the Passy-2015 field campaign main observation period (from 10 January to 28 February 2015). The grey horizontal line shows the daily average limit value of 50 μg m^{-3}. The vertical solid and dotted lines on the time series indicate the range of hourly variations of the valley heat deficit and PM_{10} concentration, respectively. The solid line on the scatter plot shows the linear regression line.

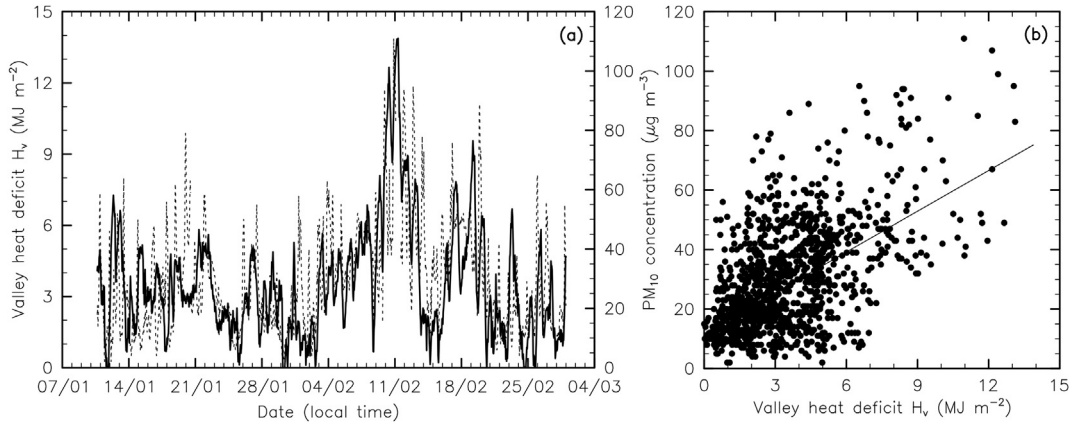

Fig. 6. (a) Time series of the hourly average valley heat deficit (solid line) and PM_{10} concentration (dotted line) at Sallanches and (b) corresponding scatter plot, during the Passy-2015 field campaign main observation period (from 10 January to 28 February 2015). The solid line on the scatter plot shows the linear regression line.

precipitation is effective in cleaning the polluted atmosphere. Large particles (with aerodynamic diameters greater than 1 μm) are most efficiently removed by washout. Hence, it is reasonable to hypothesize that low PM_{10} concentrations can be associated with washout, irrespective of the value of the valley heat deficit. Excluding the hours when precipitation occurred to eliminate such values does not reduce the scatter, leading to a similar correlation coefficient for the hourly average values ($r^2 = 0.32$ to be compared to $r^2 = 0.31$). Drawing randomly subsets of the data of the same size as that filtered for precipitation leads to correlation coefficients r^2 in the range 0.26–0.34. Hence, it is impossible to state the significance of the former change, or lack of, in r^2, except that it is within the bounds of error for the dataset.

3.2. Role of PM_{10} emissions and local dynamics on the hourly variability of PM_{10} concentrations

PM_{10} concentrations depend on PM_{10} emissions from various source sectors. The residential combustion and road transport source sectors are major source sectors for PM_{10} in the Arve River Valley in the French Alps (see Sect. 1) with 61% of annual PM_{10} emissions from residential combustion (almost exclusively wood combustion) and 23% from road transport (estimated by Air Rhône-Alpes, 2014; for 2012). Fig. 7 shows the mean hour-of-day variation of PM_{10} concentration at Sallanches during the Passy-2015 field campaign main observation period, normalized by the mean value during this period, and diurnal profiles of PM_{10} emissions for the residential combustion and road transport source sectors, and both combined, normalized by total PM_{10} emissions during the period considered. These were obtained using typical hourly and monthly emissions factors for these source sectors in France from Schaap et al. (2005) and the contributions of these source sectors to total PM_{10} emissions estimated by Air Rhône-Alpes (2014), for 2012. We note that the diurnal pattern of road transport emissions in the Arve River Valley was slightly more complicated during the period considered because heavy good vehicles were banned from the roads in this section of the valley between 2200 LT on Saturdays to 2200 LT on Sundays and from 0700 to 1800 LT on Saturdays from 7 February to 8 March 2015. Moreover, the speed limit was lowered on motorways from 130 to 110 km h^{-1} during wintertime.

The diurnal emission patterns for both source sectors are bimodal with peaks representing morning and evening peaks for residential combustion and morning and afternoon traffic rush-hour peaks for road transport. When weighted by the percentage contributions of each source sector to total PM_{10} emissions during the period considered, the diurnal emission pattern remains bimodal but follows most closely that of residential combustion. It is evident that the mean hour-of-day variation of PM_{10} concentration follows the changes in PM_{10} emissions from the residential combustion and road transport source sectors combined, despite continued PM_{10} emissions. This 'double peak' profile for PM_{10} concentration is similar to those observed elsewhere in urbanized valleys with similar mix of PM_{10} emissions during wintertime (Trompetter et al., 2010, and references therein). Reasons for the dilution of PM_{10} concentration observed between 1000 and 1700 LT (32% gradual decrease in 5 h) and between 2300 and 0700 LT (45% gradual decrease in 8 h) are explored in the following. It is worth noting that the source of dilution between 2300 and 0700 LT need not be as significant as that between 1000 and 1700 LT, since PM_{10} emissions are 2–3 times lower.

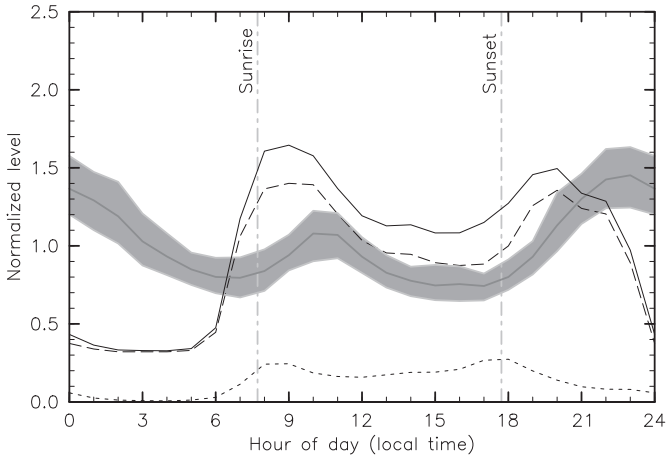

Fig. 7. Mean hour-of-day variation of PM_{10} concentration at Sallanches during the Passy-2015 field campaign main observation period (from 10 January to 28 February 2015), normalized by the mean value during this period (dark grey solid line), and diurnal profiles of PM_{10} emissions for the residential combustion (dashed line) and road transport (dotted line) source sectors, and both combined (black solid line), normalized by total PM_{10} emissions during the period considered. The 95% confidence interval for the mean hour-of-day variation of PM_{10} concentration, calculated through bootstrap re-sampling, is displayed as grey shading. The vertical lines show the average times of sunrise and sunset above the horizon during the period considered.

The *top* plot of Fig. 8 shows the mean hour-of-day variation of hourly time rate of change of the potential temperature profile derived from the MWR data during the Passy-2015 field campaign main observation period. The hourly time rate of change of the

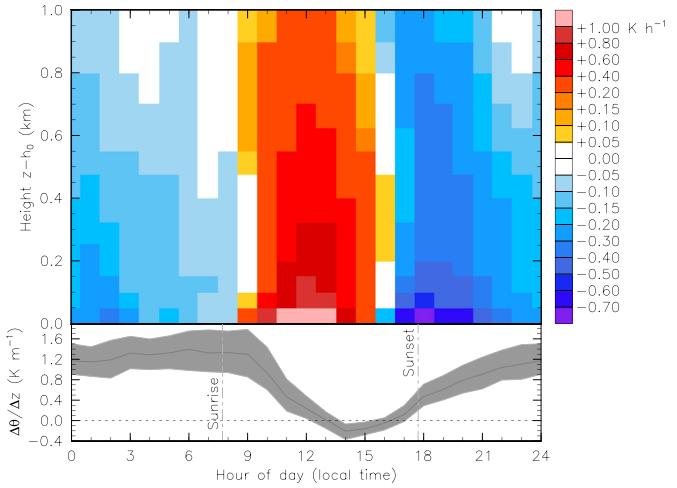

Fig. 8. The *top* plot displays the mean hour-of-day variation of hourly time rate of change of the potential temperature profile above ground level at $z = h_0$ at the location of the microwave radiometer site (see Fig. 1 and Table 1) during the Passy-2015 field campaign main observation period (from 10 January to 28 February 2015). Note that the colour scale is not linear. The *bottom* plot displays the mean hour-of-day variation of the vertical gradient of potential temperature in the first 100 m above the ground surface (dark grey solid line), denoted by $\Delta\Theta/\Delta z$, at the same location during the same period. The 95% confidence interval for the mean hour-of-day variation of $\Delta\Theta/\Delta z$, calculated through bootstrap re-sampling, is displayed as grey shading. The vertical lines shows the average times of sunrise and sunset above the horizon during the period considered. (For interpretation of the references to colour in this figure legend, the reader is referred to the web version of this article.)

potential temperature of the near-surface layer changes from negative (i.e. cooling) to positive (i.e. warming) at 0900 LT, shortly after sunrise, and increases until 1300 LT. As a result, shallow, capped boundary-layer convection develops. The vertical gradient of potential temperature in the first 100 m above the ground surface decreases during this period (see the *bottom* plot of Fig. 8), changing from positive (i.e. stable) to negative (i.e. unstable) shortly before 1300 LT, yielding a capped convective boundary layer of depth of at least 100 m at this time. Between 1400 and 1800 LT the hourly time rate of change of the potential temperature of the near-surface layer decreases, changing from warming to cooling at 1600 LT. This results in an increase of the near-surface vertical gradient of potential temperature, which changes from unstable to stable for the first 100 m around 1600 LT. Between sunset around 1800 LT and sunrise around 0800 LT the cooling rate of the near-surface layer decreases, while the near-surface vertical gradient of potential temperature continues to increase until midnight and then levels off until sunrise. This levelling off of the near-surface vertical gradient of potential temperature is associated with a progressive homogenization of the cooling rate in the vertical.

Arduini et al. (2015) found that, for an idealized alpine valley opening on a plain, the decrease of the cooling rate after the evening transition is associated with the development of the nighttime valley-wind system, characterized by drainage winds. Hence, we hypothesize that cleaner air from nighttime drainage flows dilutes the lowest layers of the valley atmosphere as the CAP grows in depth. To check whether this explanation is plausible, let us assume that this section of the valley is trapezoidal, that the slope of the valley floor is constant and that the lowest layers of the valley atmosphere above the valley floor is of depth d. Because of these simplifications, the calculation presented below does not depend on d, and so let us set d to 10 m for an illustrative purpose. Estimates of the surface area and perimeter of the valley floor are 30 km^2 and 50 km, respectively. Hence, estimates of the volume and lateral surface area of this lowest layer are 0.3 km^3 and 0.5 km^2, respectively. Let us further assume that PM_{10} concentrations are horizontally homogeneous in the valley section. Hence, the 45% gradual decrease of PM_{10} concentration between 2300 and 0700 LT, observed in Fig. 7, would require $0.3 \times 45\%$=0.135 km^3 of clean air flowing through the lateral surface area of 0.5 km^2 in 8 h, that is a wind speed in the order of 1 cm s^{-1}. If we restrict the inflow to the three major tributaries from Servoz, Saint-Gervais-les-Bains and Megève (see Fig. 1), the lateral surface area reduces to approximately 0.03 km^2, leading to a wind speed in the order of 0.2 m s^{-1}. This scenario does not lead to absurd values, suggesting that nighttime drainage flows may be key to maintaining some degree of ventilation. Furthermore, vertical transport associated with such drainage flows could provide an additional mechanism for diluting near-surface PM_{10} concentrations. The importance of these mechanisms will need to be confirmed by results from numerical model simulations. Similar conclusions were reached from observations in the Kathmandu Valley, Nepal by Panday and Prinn (2009) and confirmed by results from numerical model simulations (Panday et al., 2009).

To summarize, the interplay of the diurnal cycles of emissions and local dynamics is as follows: PM_{10} concentrations increase sharply in the morning hours shortly before sunrise and until the onset of convection due to the increase of PM_{10} emissions from proximate sources, then is diluted vertically by shallow, capped boundary-layer convection (despite continued emission), increase sharply again when convection breaks down, and then is diluted by some removal process (hypothesized drainage winds) when PM_{10} emissions are minimum.

4. Conclusions

Analysis of temperature profile and ground-based PM_{10} concentration data collected with a temporal resolution of 1 h or finer, as part of the Passy-2015 field campaign conducted around Passy in the section of the Arve River Valley between Cluses and Servoz in the French Alps during the winter season 2014–2015 led to the following main conclusions:

- The variance of daily average PM_{10} concentration explained by the daily average valley heat deficit during wintertime in this section of the Arve River Valley is consistent with that reported when correlating $PM_{2.5}$ concentration to the valley heat deficit calculated during the late night in US valleys by Silcox et al. (2012), Whiteman et al. (2014) and Green et al. (2015), and in the Grenoble valley in the French Alps by Largeron (2010) and Largeron and Staquet (2015). In addition, the correlation between daily average PM_{10} concentration and the valley heat deficit in this section of valley is found to be sensitive to the time when the valley heat deficit is calculated. It is more appropriate to calculate the valley heat deficit during the morning hours from 0600 to 1300 local time, when the correlation is comparable to that calculated using the daily average valley heat deficit. A similar result is expected for other valleys.
- The hourly variability of PM_{10} concentrations in this section of valley is more complex and cannot be explained solely by the hourly variability of the valley heat deficit. The diurnal cycle of near-surface PM_{10} concentration is affected by local PM_{10} emissions, atmospheric stability and the local dynamics of the valley atmosphere, as evidenced for other valleys (e.g. de Franceschi and Zardi, 2009; Gohm et al., 2009). It is proposed that advection and mixing by nighttime drainage flows may be responsible for the decrease of near-surface PM_{10} concentration observed at night and that vertical mixing resulting from convection leads to a decrease of near-surface PM_{10} concentration in the morning (after the morning peak of PM_{10} emissions).

Analysis of additional observations collected during the Passy-2015 field campaign will help to understand and constrain the complex relationships between particulate air pollution and atmospheric conditions in this valley and other similar valleys. Analysis of numerical model simulations, along with these additional observations, will provide insights into the role of the local dynamics of the valley atmosphere on the spatial and temporal distribution of particulate air pollution in the valley.

Acknowledgements

We wish to thank the Bureau Municipal of Sallanches for providing access to the airfield in Sallanches and that of Passy for their kind support. The rawinsonde data were collected during the Passy-2015 field campaign, supported by the Agence de l'Environnement et de la Maîtrise de l'Énergie (ADEME) through the French program Les Enveloppes Fluides et l'Environnement (LEFE), and by Météo-France. The LEFE program is managed and coordinated by the Institut National des Sciences de l'Univers (INSU) du Centre National de la Recherche Scientifique (CNRS). The Passy-2015 field campaign was led by the Centre National de Recherches Météorologiques – Groupe d'étude de l'Atmosphère Météorologique (CNRM-GAME, UMR 3589 Météo-France and CNRS) while the Laboratoire des Ecoulements Géophysiques et Industriels (LEGI, UMR 5519 UJF/CNRS/Grenoble INP) was the coordinator of the LEFE project. Rawinsondes were funded by Météo-France and LEFE/ADEME, and the Väisälä sounding system was funded by CNRS-INSU and Météo-France and operated by the CNRM-GAME team GMEI/4M. The authors would like to acknowledge the National Centre for Atmospheric Science (NCAS) Atmospheric Measurement Facility (AMF) for the use of the microwave radiometer during this project. CC would like to thank W. E. Martin and B. J. Brooks for providing technical help with the operation and deployment of this instrument. The contribution by GA to this work was supported by a grant from LabEx Osug@2020 (Investissements d'avenir – ANR10LABX56). Finally, the authors thank one referee for valuable comments, which led to substantial improvements in this paper.

References

Air Rhône-Alpes, 2014. PPA de la vallée de l'Arve: Impact du salage sur les concentrations de PM10. Technical Report. Air Rhône-Alpes, France, p. 19.

Arduini, G., Staquet, C., Chemel, C., 2015. Interactions between the night-time valley-wind system and a developing cold-air pool. Bound. Layer Meteorol. (Submitted).

Chazette, P., Couvert, P., Randriamiarisoa, H., Sanak, J., Bonsang, B., Moral, P., Berthier, S., Salanave, S., Toussaint, F., 2005. Three-dimensional survey of pollution during winter in French Alps valleys. Atmos. Environ. 39, 1035–1047.

Crewell, S., Löhnert, U., 2007. Accuracy of boundary layer temperature profiles retrieved with multifrequency multiangle microwave radiometry. IEEE Trans. Geosci. Remote Sens. 45, 2195–2201.

de Franceschi, M., Zardi, D., 2009. Study of wintertime high pollution episodes during the Brenner-South ALPNAP measurement campaign. Meteorol. Atmos. Phys. 103, 237–250.

Gohm, A., Harnisch, F., Vergeiner, J., Obleitner, F., Schnitzhofer, R., Hansel, A., Fix, A., Neininger, B., Emeis, S., Schäfer, K., 2009. Air pollution transport in an alpine valley: results from airborne and ground-based observations. Bound. Layer Meteorol. 131, 441–463.

Green, M.C., Chow, J.C., Watson, J.G., Dick, K., Inouye, D., 2015. Effect of snow cover and atmospheric stability on winter $PM_{2.5}$ concentrations in western U.S. valleys. J. Appl. Meteorol. Climatol. 54, 1191–1201.

Harnisch, F., Gohm, A., Fix, A., Schnitzhofer, R., Hansel, A., Neininger, B., 2009. Spatial distribution of aerosols in the Inn Valley atmosphere during wintertime. Meteorol. Atmos. Phys. 103, 223–235.

Lareau, N., Crosman, E., Whiteman, C.D., Horel, J.D., Hoch, S.W., Brown, W.O.J., Horst, T.W., 2013. The persistent cold-air pool study. Bull. Am. Meteorol. Soc. 94, 51–63.

Largeron, Y., 2010. Dynamique de la couche limite atmosphérique stable en relief complexe. Application aux épisodes de pollution particulaire des vallées alpines. Université de Grenoble, France. Ph.D. thesis. <tel-00606115>.

Largeron, Y., Staquet, C., 2015. Persistent inversions dynamics and wintertime PM_{10} air pollution in alpine valleys. Atmos. Environ. (Submitted).

Legain, D., Bousquet, O., Douffet, T., Tzanos, D., Moulin, E., Barrie, J., Renard, J.B., 2013. High-frequency boundary layer profiling with reusable radiosondes. Atmos. Meas. Tech. 6, 2195–2205.

Löhnert, U., Maier, O., 2012. Operational profiling of temperature using ground-based microwave radiometry at Payerne: prospects and challenges. Atmos. Meas. Tech. 5, 1121–1134.

Malek, E., Davis, T., Martin, R.S., Silva, P.J., 2006. Meteorological and environmental aspects of one of the worst national air pollution episodes (January, 2004) in Logan, Cache Valley, Utah, USA. Atmos. Res. 79, 108–122.

Paci, A., Staquet, C., 43 co-authors, 2015a. The Passy-2015 field experiment: an overview of the campaign and preliminary results. In: Proc. of the 33rd International Conference on Alpine Meteorology, Innsbruck, Austria.

Paci, A., Staquet, C., Co-authors, 2015b. The Passy-2015 field experiment: wintertime atmospheric dynamics and air quality in a narrow alpine valley. Atmos. Chem. Phys. Discuss. (In preparation).

Panday, A.K., Prinn, R.G., 2009. Diurnal cycle of air pollution in the Kathmandu Valley, Nepal: observations. J. Geophys. Res. 114, D09305.

Panday, A.K., Prinn, R.G., Schär, C., 2009. Diurnal cycle of air pollution in the Kathmandu Valley, Nepal: 2. Modeling results. J. Geophys. Res. 114, D21308.

Rampanelli, G., Zardi, D., Rotunno, R., 2004. Mechanism of up-valley winds. J. Atmos. Sci. 61, 3097–3111.

Rose, T., Crewell, S., Löhnert, U., Simmer, C., 2005. A network suitable microwave radiometer for operational monitoring of the cloudy atmosphere. Atmos. Res. 75, 183–200.

Schaap, M., Roemer, M., Sauter, F., Boersen, G., Timmermans, R., Builtjes, P.J.H., Vermeulen, A.T., 2005. LOTOS-EUROS: Documentation. TNO-report B&O-A R 2005/297. TNO, The Netherlands.

Schnitzhofer, R., Norman, M., Wisthaler, A., Vergeiner, J., Harnisch, F., Gohm, A., Obleitner, F., Fix, A., Neininger, B., Hansel, A., 2009. A multimethodological approach to study the spatial distribution of air pollution in an alpine valley during wintertime. Atmos. Chem. Phys. 9, 3385–3396.

Serafin, S., Zardi, D., 2011. Daytime development of the boundary layer over a plain and in a valley under fair weather conditions: a comparison by means of idealized numerical simulations. J. Atmos. Sci. 68, 2128–2141.

Silcox, G.D., Kelly, K.E., Crosman, E.T., Whiteman, C.D., Allen, B.L., 2012. Wintertime $PM_{2.5}$ concentrations during persistent, multi-day cold-air pools in a mountain valley. Atmos. Environ. 46, 17–24.

Staquet, C., Paci, A., 24 co-authors, 2015. The Passy project: objectives, underlying scientific questions and preliminary numerical modelling of the Passy Alpine valley. In: Proc. of the 33rd International Conference on Alpine Meteorology, Innsbruck, Austria.

Trompetter, W.J., Davy, P.,K., Markwitz, A., 2010. Influence of environmental conditions on carbonaceous particle concentrations within new zealand. J. Aerosol Sci. 41, 134–142.

Whiteman, C.D., Bian, X., Zhong, S., 1999. Wintertime evolution of the temperature inversion in the Colorado Plateau Basin. J. Appl. Meteorol. 38, 1103–1117.

Whiteman, C.D., Hoch, S.W., Horel, J.D., Charland, A., 2014. Relationship between particulate air pollution and meteorological variables in Utah's Salt Lake Valley. Atmos. Environ. 94, 742–753.

Whiteman, C.D., Zhong, S., Shaw, W.J., Hubbe, J.M., Bian, X., Mittelstadt, J., 2001. Cold pools in the Columbia basin. Weather Forecast. 16, 432–447.